Chemical reaction effect on stability and instability of double-diffusive convection in a porous medium layer: Brinkman Model

Huda A. Challoob, Fahad K.Nashmi and Akil J. Harfash
Department of Mathematics, College of Sciences, University of Basrah, Basrah, Iraq

Doi 10.29072/basjs.2018106

Aabstract

In this article, the problem of double diffusive convective in a saturated porous medium of a reacting solute using the Brinkman model has been studied. We analyze the effect of slip boundary conditions on instability and stability of this model. The linear instability and nonlinear energy stability theories are used. We analyze when stability and instability begin and determine the critical Rayleigh number as a function of the slip coefficient. Furthermore, the effect of the inclusion of the chemical reaction rate and the Brinkman coefficient on the instability and stability of the model is considered. Moreover, the effects of the inertia coefficient on the linear instability boundary have been investigated.

Keywords: Chemical reaction; Double-diffusive; porous medium; slip boundary conditions; Brinkman model.

1 Introduction

Examination of the gradients of two class agencies, such as heat and salt, with differing diffusion, simultaneously present in a fluid layer, can occur a variety of interesting convective phenomena which cannot be in a single component fluid. In the last few decades, extensive theoretical and experimental investigations have focussed upon convection in a fluid layer with two or more stratifying agencies. Turner [1-3], Huppert and Turner [4], Platten and Legros [5] have presented informative reviews of these studies. The significant difference between single component and multi-component systems has led to attention to the study of two or multi-component convection. In contrast to single component systems, convection begins even when the density decreases with height, i.e., when the basic state is hydrostatically stable. Double diffusive convection is of importance in a variety of areas such as high-quality crystal production, liquid gas storage, oceanography, pure pharmaceutical production, solidification of molten alloys, and geothermally heated lakes and magmas.

Combine chemical reaction with heat and mass transfer problems is important in a range of processes and therefore, has received considerable attention in recent years. It appears in processes such as drying, flow in a desert cooler, transfer of energy in the wet cooling tower, and evaporation of the surface of the water body. . Potential applications of this type of flow can be found in industries such as power industry, where among electric power generation methods is one in which electrical energy is extracted directly from a moving conducting fluid.

The researchers gave a lot of attention convective prolems of heat and mass transfer that are at the same time under the influence of chemical reactions because such processes are present in a variety of branches of science and technology [6-8]. This type of flow can be applied in many industries, for example in the dynamic magnetic energy generators (MHD), cooling of nuclear reactors and chemical industry. Free thermal flow occurs in nature not only because of temperature variation, but also because of concentration difference or combination of these two effect.

In industrial applications, there are many transport processes, where simultaneous heat and mass transport occur as a result of the common buoyancy effects of the spread of chemical species. Free convection in a porous medium with chemical reactions effects has many applications in geothermal and oil reservoir as well as in chemical reactors of porous structure.

The object of this paper is to study the problem of double-diffusive convection in porous media using Brinkman model. Particularly, the effect of slip boundary conditions, chemical reaction rate, and variable gravity were investigated. The interesting situation arises from a geophysical and mathematical point of view when the layer is simultaneously heated and salted from the bottom of the layer. In this case, the heating extends the fluid at the bottom of the layer and this in turn wants to rise thereby encouraging motion due to thermal convection. However, the heavy salt at the bottom of the layer has a completely opposite effect and this prevents the movement through convective overturning. Thus, these two physical effects are competing against each other. Because of this competition, the linear instability theory does not always describe the physics of instability completely and subcritica instability region may arise before the linear threshold is reached. Recent contributions to the study include instability in fluid and porous media [9-18].

The paper plan is as follows. In the next section, we present the equations of governing and derive the associated equations of disturbance. Next, we analyze the problem using the linear instability theory (Section 3) and the nonlinear stability theory (Section 4). Since stability analyses require solving the eigenvalue systems which have non-constant coefficients, these problems have to be solved numerically and an appropriate numerical method is described in Section 5. In Section 6, the numerical results of linear and nonlinear theories are presented and discussed.

2 Mathematical formulation and governing equations

Let us consider a layer Ω bounded by two horizontal planes . Let $d>0, \Omega=\mathrm{R}^2=(0,d)$ and $Oxyz$ be a Cartesian frame of reference with unit vectors i, j, k . Also, assuming that the Oberbeck-Boussinesq approximation is valid (cf. [21] and [23] and references therein), the flow in the porous medium is governed by Darcy's law

$$\tilde{\alpha} v_{i,t} = -\frac{\mu}{\kappa} v_i - p_{,i} - k_i H(z)\rho(T,C) + \tilde{\lambda}\Delta v_i, \tag{1}$$

$$v_{i,i} = 0, \tag{2}$$

$$\frac{1}{M_1} T_{,t} + v_i T_{,i} = \kappa_t \nabla^2 T, \tag{3}$$

$$\varepsilon C_{,t} + v_i C_{,i} = \kappa_c \nabla^2 C - K_1 (C - C_0), \tag{4}$$

we have denoted v , T , p, , C , H, κ, μ, K_1, C_0 , $\tilde{\lambda}$, $\tilde{\alpha}$, ε and κ_c to be the velocity, temperature, pressure, concentration, gravitational acceleration, permeability, viscosity, chemical reaction rate, reference concentration, Brinkman coefficient, inertia coefficient, porosity and salt diffusivity, respectively. The density ρ is of the form

$$\rho(T,C)=\rho_0(1-\alpha_t(T-T_0)+\alpha_c(C-C_0))$$

where ρ_0 is a reference density, T_0 is a reference temperature, α_t is a thermal expansion coefficients, and α_c is the solutal expansion coefficients. The derivation of equations (1) - (4) can be found in [21].

The fluid is subjected to the buoyancy forces resulting from temperature difference (T_L-T_U) and the diffusion of mass due to the concentration difference (C_L-C_U) between the upper and lower planes where $T_L>T_U$ and $C_L>C_U$.The steady state, for which there is no fluid flow, is given by

$$\bar{v}_i\equiv 0,\ \frac{d\bar{C}}{dz}=-\frac{\Delta C}{d}\mathsf{F}(\frac{z}{d};\xi,\eta),\ \bar{T}=-\beta z+T_L,\ \frac{d\bar{p}}{dz}=-g(z)\ \rho(\bar{T},\bar{C}),$$

where

$$\mathsf{F}(\frac{z}{d};\xi,\eta)=\frac{\xi}{\sinh(\xi)}\{1-\eta(1-\cosh(\xi))\}\cosh(\xi\frac{z}{d})-\xi\eta\sinh(\xi\frac{z}{d}),$$

$$\xi=A_1 d,A_1^2=\frac{K_1}{\kappa_c},\Delta C=|C_L-C_U|,\Delta T=|T_L-T_U|,\eta=\frac{C_L}{\Delta C},\beta=\frac{\Delta T}{d}.$$

To investigate the stability of these solutions, we introduce perturbations (u_i,p,θ,ϕ) by

$$v_i=u_i+\bar{v}_i,\quad p=\mathsf{P}+\bar{p},\quad T=\theta+\bar{T},\quad C=\phi+\bar{C}.$$

The perturbation equations are nondimensionalized according to the scales (stars denote dimensionless quantities)

$$x=x^*d,\ t=t^*\frac{\rho_0\kappa}{\mu},\ u=Uu^*,\ \theta=T^{\#}\theta^*,\ \phi=C^{\#}\phi^*,\ \mathsf{P}=P\mathsf{P}^*,$$

$$C^{\#}=U\sqrt{\frac{\mu d\Delta C}{\rho_0\kappa_c\alpha_c\kappa}},\ R_c=\sqrt{\frac{\kappa\rho_0\alpha_c d\Delta C}{\mu\kappa_c}},\ T^{\#}=U\sqrt{\frac{d^2\mu\beta}{\kappa\rho_0\kappa_t\alpha_t}},$$

$$R_t=\sqrt{\frac{d^2\kappa\rho_0\beta\alpha_t}{\mu\kappa_t}},\ \varepsilon^{\wedge}=\frac{1}{\varepsilon},\ U=\frac{d\mu}{\kappa\rho_0},\ P=\frac{d\mu}{\kappa}U,$$

$$p_r=\frac{d^2\mu}{M_1\kappa\rho_0\kappa_t},\ p_s=\frac{\varepsilon d^2\mu}{\kappa\rho_0\kappa_c}.$$

where p_t and p_s are the thermal and solute Prandtl numbers and R_t^2 and R_c^2 are the thermal and solute Rayleigh numbers, respectively. The dimensionless perturbation equations are (after omitting all stars)

$$\alpha u_{i,t}=-u_i-p_{,i}+R_t k_i H(z)\theta-R_c k_i H(z)\phi+\lambda\Delta u_i, \tag{5}$$

$$u_{i,i}=0, \tag{6}$$

$$p_r(\theta_{,t}+M_1 u_i\theta_{,i})=R_t w+\nabla^2\theta, \tag{7}$$

$$p_s(\phi_{,t}+\overset{\wedge}{\varepsilon}u_i\phi_{,i})=R_c\mathsf{F}(z)w+\nabla^2\phi-\xi^2\phi, \tag{8}$$

with $w=u_3$, α and λ are non-dimensional equivalents of $\tilde{\alpha}$ and $\tilde{\lambda}$, respectively, and

$$\mathsf{F}(z)=\frac{\xi}{\sinh(\xi)}\{1+\eta(1-\cosh(\xi))\}\cosh(\xi z)+\xi\eta\sinh(\xi z).$$

These equations hold on $\{z\in(0,1)\}\times\{(x,y)\in\mathsf{R}^2\}$. In (5)-(8), we select $H(z)=1-\varepsilon z$. Since the fluid is incompressible we have that $w_{,z}=-(u_{,x}+v_{,y})$. Therefore $w_{,zz}=-(u_{,xz}+v_{,yz})$, and from the boundary conditions on u and v we see that w satisfies

$$w=\theta=\phi=0,\quad w_{,z}=N_L w_{,zz}\quad \text{at}\quad z=0, \tag{9}$$

$$w=\theta=\phi=0,\quad w_{,z}=-N_U w_{,zz}\quad \text{at}\quad z=1, \tag{10}$$

In (9) and (10), N_U and N_L are dimensionless parameters of λ_U and λ_L, respectively.

3 Linear instability

In order to study linear instability, we discard the nonlinear terms in (5)-(8). A time dependence such as $u_i=e^{\sigma t}u_i(\mathbf{x}),\pi=e^{\sigma t}\pi(\mathbf{x}),\theta=e^{\sigma t}\theta(\mathbf{x}),\phi=e^{\sigma t}\phi(\mathbf{x})$ is now assumed and then, after removing, the pressure perturbation the linearized instability equations that arise from (5)-(8) are found to be

$$\sigma\alpha\Delta w=-\Delta w+R_t H(z)\Delta^*\theta-R_c H(z)\Delta^*\phi+\lambda\Delta^2 w, \tag{11}$$

$$\sigma p_r\theta=R_t w+\nabla^2\theta, \tag{12}$$

$$\sigma p_s\phi=R_c\mathsf{F}(z)w+\nabla^2\phi-\xi^2\phi, \tag{13}$$

where $\Delta^*=\partial^2/\partial x^2+\partial^2/\partial y^2$, and (11) hold on $\mathsf{R}^2\times(0,1)$. To proceed from equations (11), a plane tiling form $h(x,y)$ is introduced, see e.g. [23, 24]), and then we put $w=W(z)h(x,y)$, $\theta=\Theta(z)h(x,y)$ and $\phi=\Phi(z)h(x,y)$ and introduce the wavenumber a by $\Delta^*h=-a^2h$. Equations (11)-(13) then yield the following eigenvalue problem

$$\begin{gathered}\lambda(D^2-a^2)^2W-(D^2-a^2)W-a^2R_tH(z)\Theta+a^2R_cH(z)\Phi=\sigma\alpha(D^2-a^2)W,\\(D^2-a^2)\Theta+RW=\sigma p_r\Theta,\\(D^2-a^2-\xi^2)\Phi+R_cF(z)W=p_s\sigma\Phi,\end{gathered}$$

(14)

where $D=d/dz$. In (14), $z\in(0,1)$, and the boundary conditions are

$$\begin{gathered}\Theta=\Phi=W=DW-N_LD^2W=0,\ \text{at}\quad z=0,\\\Theta=\Phi=W=DW+N_UD^2W=0,\ \text{at}\quad z=1.\end{gathered} \tag{15}$$

Detailed numerical results are presented in Section 6.

4 Nonlinear energy stability theory

When linear analysis is adopted, it is assumed that the perturbation to the steady state is small, so the nonlinear terms are eliminated from the set of partial differential equations. Linear analysis has often proved to provide little information about the behavior of the nonlinear system

[23]. In such cases, instability can only be derived from linear thresholds, as any potential growth in nonlinear terms is not considered.

Let V be a period cell for a disturbance to (5)-(8), and let $\|\cdot\|$ and $\langle\cdot,\cdot\rangle$ be the inner product and norm on $L^2(V)$. Next, multiply (5), (7) and (8) by u_i, θ and ϕ and integrating over V ,we obtain

$$\frac{\alpha}{2}\frac{d}{dt}\|\mathbf{u}\|^2 = -\|\mathbf{u}\|^2 - \lambda\|\nabla\mathbf{u}\|^2 + \int_V R_t k_i H(z) u_i \theta dV - \int_V R_c k_i H(z) u_i \phi dV + \lambda\int_{\partial\Omega} n_j u_i u_{i,j} dS, \tag{16}$$

$$\frac{p_r}{2}\frac{d}{dt}\|\theta\|^2 = \int_V R_t w\theta dV - \|\nabla\theta\|^2, \tag{17}$$

and

$$\frac{p_s}{2}\frac{d}{dt}\|\phi\|^2 = \int_V R_c \mathsf{F}(z) w dV - \|\nabla\phi\|^2 - \xi^2\|\phi\|^2. \tag{18}$$

By introducing a coupling parameters $\lambda_1, \lambda_2 > 0$ we may then derive

$$\frac{dE}{dt} = I - D, \tag{19}$$

where the functions E and I are given by

$$E(t) = p_r\frac{\lambda_1}{2}\|\theta\|^2 + p_s\frac{\lambda_2}{2}\|\phi\|^2 + \frac{\alpha}{2}\|\mathbf{u}\|^2, \tag{20}$$

and

$$I = R_t\langle\Psi_1(z)\theta, w\rangle - R_c\langle\Psi_2(z)\theta, w\rangle, \tag{21}$$

with the dissipation D being defined by

$$D = \lambda_1\|\nabla\theta\|^2 + \|\mathbf{u}\|^2 + \lambda_2\|\nabla\phi\|^2 + \lambda_2\xi^2\|\phi\|^2 + \lambda\|\nabla\mathbf{u}\|^2 + \frac{\lambda}{N_L}\int_{\partial\Omega_L}|\mathbf{u}|^2\, dS + \frac{\lambda}{N_U}\int_{\partial\Omega_U}|\mathbf{u}|^2\, dS, \tag{22}$$

where dS is a surface element, $\Psi_1(z) = H(z) + \lambda_1$, $\Psi_2(z) = H(z) - \lambda_2\mathsf{F}(z)$ and $\mathbf{u}$ is explicitly written as $\mathbf{u} = (u, v, w)$. Define R_E by

$$\frac{1}{R_E} = \max_H \frac{I}{D}, \tag{23}$$

where H is the space of admissible functions, i.e. $u_i, \theta, \phi \in H^1(V)$ with u_i solenoidal and u_i, θ, ϕ satisfying the boundary conditions. Then from (19) we derive

$$\frac{dE}{dt} \le -D(1 - \frac{1}{R_E}). \tag{24}$$

We now are required to show that provided $R_E > 1$, then $E(t)$ decays to zero for all $E(0)$ (i.e. the perturbations $\mathbf{u}$, θ , ϕ will decay for all initial data $\mathbf{u}_0$, θ_0 , ϕ_0). If we let $\varsigma_1 = \{N_L^{-1}, N_U^{-1}, \lambda_1, \lambda_2, \lambda_2\xi^2, \lambda\}$ and $\varsigma_2 = (1 - \frac{1}{R_E})$

then from (24) we have the inequality

$$\frac{dE}{dt} \le \varsigma_1\varsigma_2(\|\mathbf{u}\|^2 + \|\phi\|^2 + \|\nabla\theta\|^2 + \|\nabla\phi\|^2 + \|\nabla\mathbf{u}\|^2 + \int_{\partial\Omega_L} |\mathbf{u}|^2\, dS + \int_{\partial\Omega_U} |\mathbf{u}|^2\, dS). \tag{25}$$

We now make use of the following Poincare's inequalities. For some $(\eta_u, \eta_\theta, \eta_\phi) \in [0,\infty)\times[0,\infty)\times[0,\infty)$ it holds that

$$\begin{gathered}\eta_u\|\mathbf{u}\|^2 \le \|\nabla\mathbf{u}\|^2 + \int_{\partial\Omega_L} |\mathbf{u}|^2\, dS + \int_{\partial\Omega_U} |\mathbf{u}|^2\, dS,\\ \eta_\theta\|\theta\|^2 \le \|\nabla\theta\|^2, \quad \eta_\phi\|\phi\|^2 \le \|\nabla\phi\|^{2^2}.\end{gathered} \tag{26}$$

Applying (26) to (25), and letting $\varsigma_3 = \min\{\eta_u, \eta_\theta, \eta_\phi\}$, we obtain

$$\begin{aligned}\frac{dE}{dt} &\le -\varsigma_1\varsigma_2\varsigma_3(\|\theta\|^2 + 2\|\phi\|^2 + 2\|\mathbf{u}\|^2) \\ &\le -\varsigma_1\varsigma_2\varsigma_3(\|\theta\|^2 + \|\phi\|^2 + \|\mathbf{u}\|^2)\end{aligned} \tag{27}$$

Finally, setting $\varsigma_4 = 2\min\{\lambda_1^{-1}p_r^{-1}, \lambda_2^{-1}p_s^{-1}, \alpha^{-1}\}$ we obtain from (22)

$$\frac{dE}{dt} \le -\varsigma_1\varsigma_2\varsigma_3\varsigma_4(\frac{\lambda_1}{2}p_r\|\theta\|^2 + \frac{\lambda_2}{2}p_s\|\phi\|^2 + \frac{\alpha}{2}\|\mathbf{u}\|^2) = -\varsigma E(t), \tag{28}$$

where $\varsigma = \varsigma_1\varsigma_2\varsigma_3\varsigma_4 > 0$, provided $R_E > 1$. This may be integrated to yield

$$E(t) \le e^{-ct}E(0). \tag{29}$$

Therefore the condition $R_E > 1$ is sufficient to ensure that all perturbations in D decay at least exponentially as time evolves and hence $R_E = 1$ gives a stability boundary. It is left for us to perform the maximization necessary to find R_E, as defined in (23). If the quotient $\frac{I(\mathbf{u},\theta,\phi)}{D(\mathbf{u},\theta,\phi)}$ is at a maximum, i.e. $\mathbf{u}$, θ and ϕ have been optimally chosen in H, then for all $(\mathbf{h},\psi,\varphi) \in H$ we have that

$$\frac{d}{d\tau}\left(\frac{I(\mathbf{u}+\tau\mathbf{h},\theta+\tau\psi,\phi+\tau\varphi)}{D(\mathbf{u}+\tau\mathbf{h},\theta+\tau\psi,\phi+\tau\varphi)}\right)\Big|_{\tau=0} = 0. \tag{30}$$

Using the quotient rule, and assuming $\frac{I}{D}$ is at a maximum, we obtain

$$\begin{aligned}\frac{d}{d\tau}\left(\frac{I(\mathbf{u}+\tau\mathbf{h},\theta+\tau\psi,\phi+\tau\varphi)}{D(\mathbf{u}+\tau\mathbf{h},\theta+\tau\psi,\phi+\tau\varphi)}\right)\Big|_{\tau=0} &= \frac{1}{D(\mathbf{u},\theta,\phi)}\Big(\frac{d}{d\tau}I(\mathbf{u}+\tau\mathbf{h},\theta+\tau\psi,\phi+\tau\varphi)\big|_{\tau=0} \\ &\quad - \frac{I(\mathbf{u},\theta,\phi)}{D(\mathbf{u},\theta,\phi)}\frac{d}{d\tau}D(\mathbf{u}+\tau\mathbf{h},\theta+\tau\psi,\phi+\tau\varphi)\big|_{\tau=0}\Big) \\ &= \frac{1}{D(\mathbf{u},\theta,\phi)}\Big(\frac{d}{d\tau}I(\mathbf{u}+\tau\mathbf{h},\theta+\tau\psi,\phi+\tau\varphi)\big|_{\tau=0} - \frac{1}{R_E}\frac{d}{d\tau}D(\mathbf{u}+\tau\mathbf{h},\theta+\tau\psi,\phi+\tau\varphi)\big|_{\tau=0}\Big) \\ &= \frac{1}{D(\mathbf{u},\theta,\phi)}\Big(\frac{d}{d\tau}I(\mathbf{u}+\tau\mathbf{h},\theta+\tau\psi,\phi+\tau\varphi)\big|_{\tau=0} - \frac{d}{d\tau}D(\mathbf{u}+\tau\mathbf{h},\theta+\tau\psi,\phi+\tau\varphi)\big|_{\tau=0}\Big),\end{aligned}$$

and so $\frac{I}{D}$ is at a maximum provided that

$$\frac{d}{d\tau}I(\mathbf{u}+\tau\mathbf{h},\theta+\tau\psi,\phi+\tau\varphi)|_{\tau=0}-\frac{d}{d\tau}D(\mathbf{u}+\tau\mathbf{h},\theta+\tau\psi,\phi+\tau\varphi)|_{\tau=0}=0. \quad (31)$$

Calculating the above derivatives,

$$\frac{d}{d\tau}I(\mathbf{u}+\tau\mathbf{h},\theta+\tau\psi,\phi+\tau\varphi)|_{\tau=0}=R_t(k_i\theta\psi_1(z),h_i)+R_t(w\psi_1(z),\psi)$$
$$-R_c(k_i\phi\psi_2(z),h_i)-R_c(w\psi_2(z),\varphi)$$
$$=k_i(R_t\theta\psi_1(z),-R_c\phi\psi_2(z),h_i)+(R_t(w\psi_1(z),\psi),h_i)-R_c(w\psi_2(z),\varphi),$$
$$\frac{d}{d\tau}D(\mathbf{u}+\tau\mathbf{h},\theta+\tau\psi,\phi+\tau\varphi)|_{\tau=0}=-2\lambda_1(\Delta\theta,\psi)-2\lambda_2(\Delta\phi,\varphi)$$
$$+2(u_i,h_i)+2\lambda_2\xi^2(\phi,\varphi)-2\lambda(\Delta u,h_i)+\lambda\int_{\partial\Omega}u_{i,j}h_in_jdS-\lambda\int_{\partial\Omega}u_ih_{i,j}n_jdS$$

Once more, the surface integrals vanish on $\partial\Omega\backslash\{\partial\Omega_L\cup\partial\Omega_U\}$, owing to the periodicity of $\mathbf{h},\psi$ and φ, while the surface integral of $\psi\theta_{,i}$ and $\varphi\phi_{,i}$ vanish altogether. Therefore, applying the boundary conditions on $\mathbf{u}$ and $\mathbf{h}$ at Ω_L and Ω_U,

$$\int_{\partial\Omega}u_{i,j}h_in_jdS-\int_{\partial\Omega}u_ih_{i,j}n_jdS=\int_{\partial\Omega}(u_{i,j}h_i-u_ih_{i,j})n_jdS$$
$$=\int_{\partial\Omega_U}(u_{i,j}h_i-u_ih_{i,j})n_jdS+\int_{\partial\Omega_L}(u_{i,j}h_i-u_ih_{i,j})n_jdS$$
$$=-\int_{\partial\Omega_U}\frac{1}{N_L}(u_ih_i-u_ih_i)dS-\int_{\partial\Omega_L}\frac{1}{N_U}(u_ih_i-u_ih_i)dS=0.$$

Therefore

$$\frac{d}{d\tau}D(\mathbf{u}+\tau\mathbf{h},\theta+\tau\psi,\phi+\tau\varphi)|_{\tau=0}=-2\lambda_1(\Delta\theta,\psi)-2\lambda_2(\Delta\phi,\varphi)$$
$$+2(u_i,h_i)+2\lambda_2\xi^2(\phi,\varphi)-2\lambda(\Delta u,h_i)$$

We include the conditions $h_{i,i}=0$ by way of a Lagrange multiplier $\zeta(\mathbf{x})$,

$$(h_{i,i},\zeta)=((h_i\zeta)_{,i},1)-(h_i,\zeta_{,i})=-(h_i,\zeta_{,i}).$$

Finally, grouping all our terms in h_i,ψ and φ, we obtain for equation (31)

$$((2\lambda\Delta u_i-2u+R_tk_i\psi_1(z)\theta-R_ck_i\psi_2(z)\phi),h_i) \quad (32)$$
$$+((2\lambda_1\Delta\theta+R_t\psi_1(z)w),\psi)+((2\lambda_2\Delta\phi-2\lambda_2\xi^2-R_c\psi_2(z)w),\varphi)=0.$$

The functions $\mathbf{h},\psi$ and φ were chosen arbitrarily from H. Therefore, in general, we must have

$$\begin{gathered}2\lambda\Delta^2u_i-2u_i+R_tk_i\Psi_1\theta-R_ck_i\Psi_2\phi=\zeta_{,i},\\ R_t\Psi_1w+2\lambda_1\Delta\theta=0,\quad 2\lambda_2\Delta\phi-2\lambda_2\xi^2\phi-R_c\Psi_2w=0,\end{gathered} \quad (33)$$

where ζ is a lagrange multiplier. To remove the lagrange multiplier we take the third component of the double *curl* of $(23)_1$, and introducing the normal mode representation and notation as presented in Section 3, thus (23) then becomes

$$\begin{gathered}\lambda(D^2-a^2)^2W-2(D^2-a^2)W+a^2R_c\Psi_2\Phi=a^2R_t\Psi_1\Theta,\\ 2\lambda_1(D^2-a^2)\Theta+R_t\Psi_1W=0,\quad 2\lambda_2(D^2-a^2-\xi^2)\Phi-R_c\Psi_2W=0,\end{gathered} \quad (34)$$

together with boundary conditions (15). Then, the critical Rayleigh Ra_E we can evaluate by fixing a^2, λ_1 and λ_2, then, we utilize the golden section search to minimize Ra_E for a^2 and then maximize Ra_E for λ_1 and λ_2 to compute Ra_E for nonlinear stability theory, from

$$Ra_E = \max_{\lambda_1,\lambda_2} \min_{a^2} R^2(a^2,\lambda_1,\lambda_2), \tag{35}$$

where we have stability for all $R^2 < Ra_E$. The numerical results have been introduced in the following section and compared with linear instability theory. Numerical results of nonlinear thresolds have been introduced in Section 6.

5 Numerical technique

In this section, we use the Chebyshev collocation method to solve the eigenvalue system (21) and (41). The eigenvalue systems (14) and (34) have been solved using the Chebyshev collocation method, for more details [6-18].

In the Chebyshev collocation method, system (14) is rewritten in terms of second and third order derivatives only. Letting $\Pi = DW$, (14) can be expressed as the four 2nd order equations. The system is then transformed onto the Chebyshev domain $(-1,1)$ and the solutions W and θ treated as independent variables and expanded in a series of Chebyshev polynomials

$$W = \sum_{n=0}^{N} w_n T_n(z),\quad \Pi = \sum_{n=0}^{N} \Pi_n T_n(z),\quad \Theta = \sum_{n=0}^{N} \Theta_n T_n(z), \Phi = \sum_{n=0}^{N} \Phi_n T_n(z), \tag{36}$$

then, we insert (36) into the equations (14), and then substitute the Gauss-Labatto points which are defined by

$$y_i = \cos\left(\frac{\pi i}{N-3}\right),\ i = 0,\ldots,N-2. \tag{37}$$

Thus, we obtain $4N-4$ algebraic equations for $4N+4$ unknowns $W_0,\ldots,W_N$, $\Pi_0,\ldots,\Pi_N$, $\Theta_0,\ldots,\Theta_N$, $\Phi_0,\ldots,\Phi_N$. Now, we can add six rows using the boundary conditions (15) as follows

$$BC_1 : \sum_{n=0}^{N} W_n = 0,\quad BC_2 : \sum_{n=0}^{N} (-1)^n W_n = 0,\quad BC_3 : \sum_{n=0}^{N} n^2 N_U \Pi_n + \Pi_n = 0,$$

$$BC_4 : \sum_{n=0}^{N} (-1)^{n+1} n^2 N_U \Pi_n - (-1)^n \Pi_n = 0,\quad BC_5 : \sum_{n=0}^{N} \Theta_n = 0,$$

$$BC_6 : \sum_{n=0}^{N} (-1)^n \Theta_n = 0,\quad BC_7 : \sum_{n=0}^{N} \Phi_n = 0,\quad BC_8 : \sum_{n=0}^{N} (-1)^n \Phi_n = 0.$$

Using the above notations, we can obtain the following generalised eigenvalue problem:

$$\begin{pmatrix} 2D & -I & O & O \\ BC_1 & 0...0 & 0...0 & 0...0 \\ BC_2 & 0...0 & 0...0 & 0...0 \\ \Omega_0 & \Omega_1 & -a^2R_t\Sigma & a^2R_c\Sigma \\ 0...0 & BC_3 & 0...0 & 0...0 \\ 0...0 & BC_4 & 0...0 & 0...0 \\ R_tI & O & \Omega_2 & O \\ 0...0 & 0...0 & BC_5 & 0...0 \\ 0...0 & 0...0 & BC_6 & 0...0 \\ R_cI & O & O & \Omega_3 \\ 0...0 & 0...0 & 0...0 & BC_7 \\ 0...0 & 0...0 & 0...0 & BC_8 \end{pmatrix} X = \sigma \begin{pmatrix} O & O & O & O \\ 0...0 & 0...0 & 0...0 & 0...0 \\ 0...0 & 0...0 & 0...0 & 0...0 \\ -a^2\alpha I & 2\alpha D & O & O \\ 0...0 & 0...0 & 0...0 & 0...0 \\ 0...0 & 0...0 & 0...0 & 0...0 \\ O & O & I & O \\ 0...0 & 0...0 & 0...0 & 0...0 \\ 0...0 & 0...0 & 0...0 & 0...0 \\ O & O & O & p_sI \\ 0...0 & 0...0 & 0...0 & 0...0 \\ 0...0 & 0...0 & 0...0 & 0...0 \end{pmatrix} X, \qquad (38)$$

where $X = (W_0,...,W_N, \Theta_0,...,\Theta_N, \Phi_0,...,\Phi_N)$, O is the zeros matrix,

$I(n_1,n_2) = T_{n_2}(z_{n_1})$,

$D(n_1,n_2) = T'_{n_2}(z_{n_1})$,

$D^2(n_1,n_2) = T''_{n_2}(z_{n_1})$,

$\Sigma(n_1,n_2) = H(z_{n_1})I(n_1,n_2)$,

$\Omega_0 = \lambda a^4 I(n_1,n_2) + a^2 I(n_1,n_2)$,

$\Omega_1 = \lambda(8D^3(n_1,n_2) - 4a^2 D(n_1,n_2)) - 2D(n_1,n_2)$,

$\Omega_2 = 4D^2(n_1,n_2) - a^2 I(n_1,n_2)$,

$\Omega_3 = 4D^2(n_1,n_2) - (a^2 + \xi^2) I(n_1,n_2)$,

$n_1 = 0,...,N-2$ and $n_2 = 0,...,N$.

We computed the differentiation matrices, which are corresponded to the trail functions (38) analytically using Matlab routines.

We have solved system (38) for eigenvalues σ_j by using the QZ algorithm from Matlab routines. Once the eigenvalues σ_j are found we use the secant method to locate where σ_j^R, $\sigma_j = \sigma_j^R + \sigma_j^I$ being the real and imaginary parts of eigenvalue σ_j. The value of R which makes $\sigma_1^R = 0$, σ_1^R being the largest eigenvalue, is the critical value of R for a^2 fixed. We then use golden section search to minimize over a^2 and find the critical value of R^2 for linear instability. Numerical results are reported in the next section. In our use of the Chebyshev collocation method, we used polynomial of degree between 20 and 30. Usually 25 was found to be sufficient but convergence was checked by varying the degree by examining the convergence of the associated eigenvector (which yields the approximate associated eigenfunction).

Returning to the nonlinear eigenvalue system (41), the the Chebyshev collocation method yields:

$$\begin{pmatrix} 2D & -I & O & O \\ BC_1 & 0...0 & 0...0 & 0...0 \\ BC_2 & 0...0 & 0...0 & 0...0 \\ \Omega_0 & \Omega_1 & O & 0.5a^2R_c\Lambda_2 \\ 0...0 & BC_3 & 0...0 & 0...0 \\ 0...0 & BC_4 & 0...0 & 0...0 \\ O & O & 2\lambda_1\Omega_2 & O \\ 0...0 & 0...0 & BC_5 & 0...0 \\ 0...0 & 0...0 & BC_6 & 0...0 \\ -R_c\Lambda_2 & O & O & 2\lambda_2\Omega_3 \\ 0...0 & 0...0 & 0...0 & BC_7 \\ 0...0 & 0...0 & 0...0 & BC_8 \end{pmatrix} X = R_t \begin{pmatrix} O & O & O & O \\ 0...0 & 0...0 & 0...0 & 0...0 \\ 0...0 & 0...0 & 0...0 & 0...0 \\ O & O & 0.5a^2\Lambda_1 & O \\ 0...0 & 0...0 & 0...0 & 0...0 \\ 0...0 & 0...0 & 0...0 & 0...0 \\ -\Lambda_1 & O & O & O \\ 0...0 & 0...0 & 0...0 & 0...0 \\ 0...0 & 0...0 & 0...0 & 0...0 \\ O & O & O & O \\ 0...0 & 0...0 & 0...0 & 0...0 \\ 0...0 & 0...0 & 0...0 & 0...0 \end{pmatrix} X, \quad (39)$$

where

$$\Lambda_1(n_1,n_2) = (\lambda_1 + H(z_{n_1}))I(n_1,n_2),$$
$$\Lambda_2(n_1,n_2) = (H(z_{n_1}) - \lambda_2 \mathsf{F}(z))I(n_1,n_2).$$

Then, the critical Rayleigh Ra_E we can evaluate by fixing a^2, λ_1 and λ_2, then, we utilize the golden section search to minimize Ra_E for a^2 and then maximize Ra_E for λ_1 and λ_2 to compute Ra_E for nonlinear stability theory, from

$$Ra_E = \max_{\lambda_1,\lambda_2} \min_{a^2} R^2(a^2,\lambda_1,\lambda_2), \quad (40)$$

where we have stability for all $R^2 < Ra_E$. The numerical results have been introduced in the following section and compared with linear instability theory.

6 Stability analysis results

The numerical results are presented for $H(z) = 1 - \varepsilon z$ and $N_L = N_U = N_0$. To study the possibility of a wide-scale gravitational field (sign can also be change) we select ε to vary from 0 to 1. In this paper, the results are introduced for $N_L = N_U = N_0$, $M_1 = 1$, $p_r = 1$ and $p_s = 5$.

The linear instability and nonlinear stability thresholds are presented in Figure 1. If the linear theory is achieved by stationary convection, we note the convergence between the linear and nonlinear thresholds. However, this relationship of convergence will not continue as the solute

Rayleigh number increases, which show that the linear theory may fail to simulate physics appropriately of the onset of convection. The behavior of linear instability curves is perfectly consistent with what we have seen [25]. The kink in the curves represents the point at which convection switches from steady convection ($\sigma = 0$) to oscillatory ($\sigma_r = 0, \sigma_i \neq 0$). Note that for small values R_c the stationary mode appears in the linear instability, however, as R_c increases the oscillatory mode become present in the linear instability thresholds. Figure 1 confirms that the increase in values of R_c leads to an increase in the values of the critical Rayleigh number which confirms the stabilising effect of R_c.

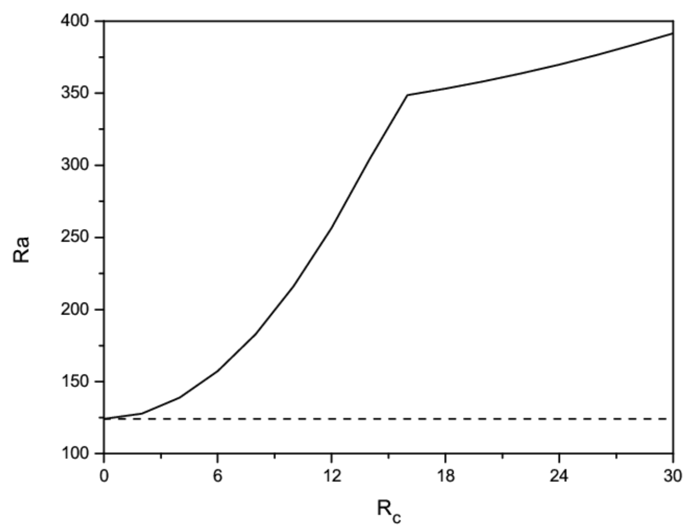

Figure 1: : The critical thermal Rayleigh number of linear theory (solid line) and nonlinear theory (dashed line) plotted against the solute Rayleigh number R_c, where $\varepsilon = \lambda = 0.1$ and $\alpha = N_0 = \xi = \eta = 1$.

Figure 2 explains the linear instability and nonlinear stability thresholds, with critical thermal Rayleigh number Ra plotted against ε .where $\lambda = 0.1$, $\alpha = N_0 = \xi = \eta = 1$ and $R_c = 20$. In this figure, with small values of ε. It is clear that the linear and nonlinear thresholds have an acceptable relationship, indicating the appropriateness of linear theory to predict the physics of the onset of convection. With increased the value of ε these thresholds have a lower correlation. It is interesting to note that the oscillation mode is presented at linear instability thresholds when $\varepsilon \leq 0.8$, otherwise, the stationary mode appears in linear instability.

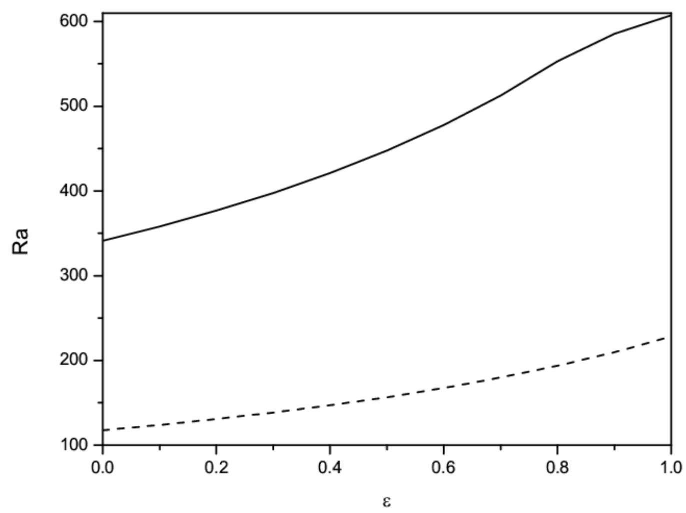

Figure 2: The critical thermal Rayleigh number of linear theory (solid line) and nonlinear theory (dashed line) plotted against ε, where $\lambda = 0.1$, $\alpha = N_0 = \xi = \eta = 1$ and $R_c = 20$.

Figure 3 shows critical linear and nonlinear boundaries for a variety values of λ. In this figure, we note that an increase in λ values makes the system to become more stable. Since the results of linear instability and nonlinear stability show not good agreement, we conclude that (for the ranges of the parameters explored), the linear theory does not accurately cover the physics of the onset of convection. Thus, the results of instability are supported by a large area of subcritical instability. However, for a fixed value of $\varepsilon = 0.1$, $\alpha = N_0 = \xi = \eta = 1$ and $R_c = 20$, we see that oscillatory convection is occurring for $\lambda \le 0.7$ and when $\lambda > 0.7$ we shall witness stationary convection.

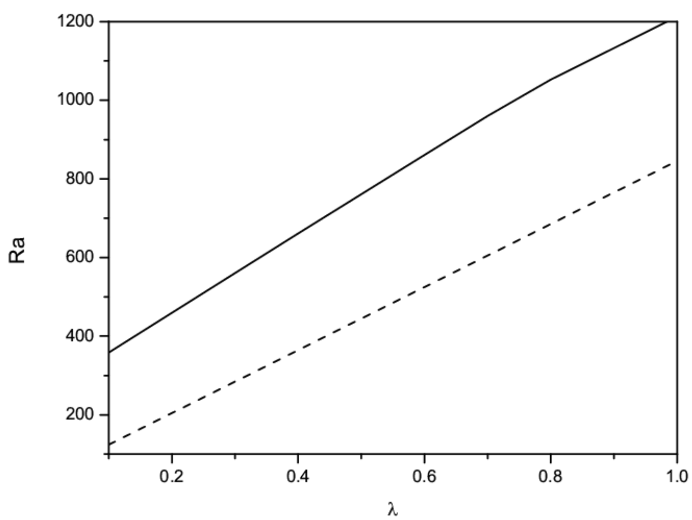

Figure 3: The critical thermal Rayleigh number of linear theory (solid line) and nonlinear theory (dashed line) plotted against λ, where $\varepsilon = 0.1$, $\alpha = N_0 = \xi = \eta = 1$ and $R_c = 20$.

In Figure 4,we display the critical Rayleigh numbers at which stability and instability begin as a function of the slip coefficient, N_0. From Figure 4, it is clear that the region of subcritical instabilities between the linear and nonlinear thresholds is very large. Also in this figure, we note that the instability curve always lies below the stationary convection one and thus the oscillatory convection is always dominant, for the fixed value of ε, λ, α, ξ, η and R_c.

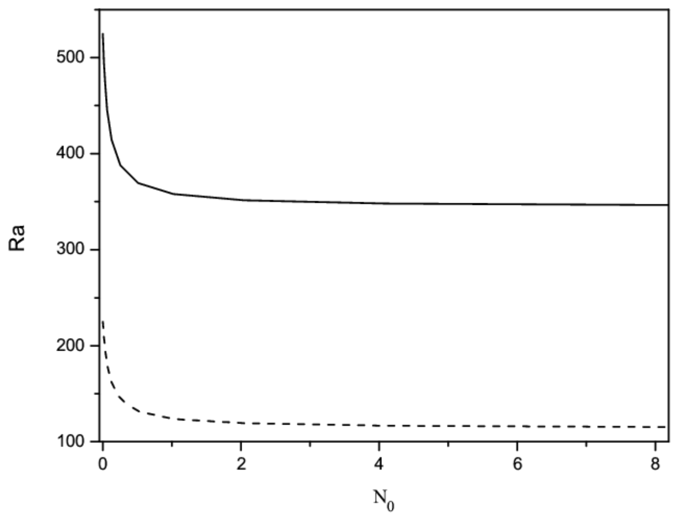

Figure 4: The critical thermal Rayleigh number of linear theory (solid line) and nonlinear theory (dashed line) plotted against N_0, where $\varepsilon = \lambda = 0.1$, $\alpha = \xi = \eta = 1$ and $R_c = 20$.

Figure 5 shows the effect ξ on critical Rayleigh numbers of linear and nonlinear theories. This figure shows that the increasing in ξ value leads to make the system more stable, which is physically expect. Moreover, note that the oscillatory convection is always dominant as for all critical values of σ we have $\sigma_i \neq 0$.

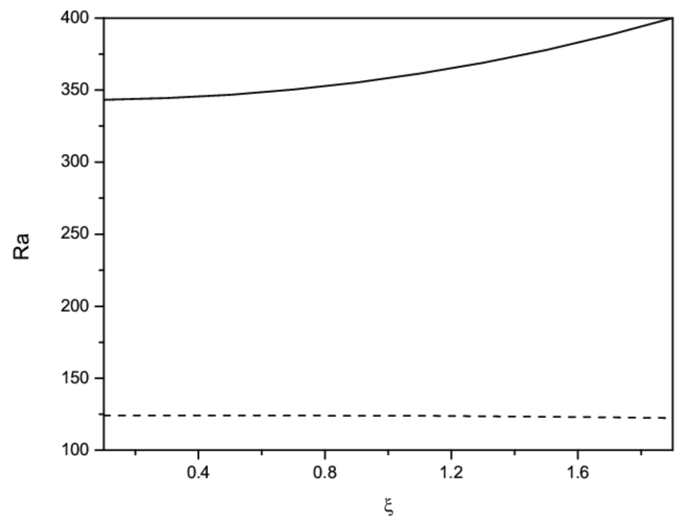

Figure 5: The critical thermal Rayleigh number of linear theory (solid line) and nonlinear theory (dashed line) plotted against ξ, where $\varepsilon = \lambda = 0.1$, $\alpha = N_0 = \eta = 1$ and $R_c = 20$.

A visual representation of the linear instability and global nonlinear stability thresholds is given in Figure 6. In Figure 6 the spectrum of σ is found numerically to always be not real and hence the nature of convection was always oscillatory. Figure 6 shows the stabilizing effect of increasing η. The decrease in Ra in Figure 6, is to be expected due to the definition of η. For example, $\eta = 0.5$ corresponds to $c_L = -c_U$. If we take $\eta = 0.6$ this corresponds to $c_L = -3c_L/2$. The coefficient of c_L increases as η increases and this means that the stabilizing effect due to heavier fluid above is lessening.

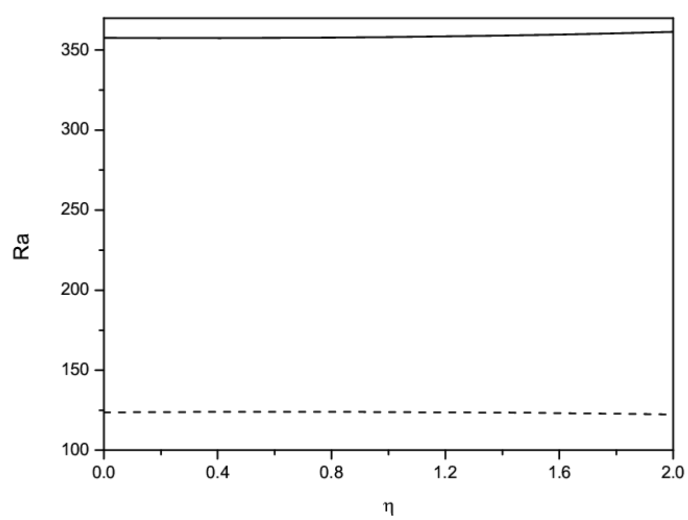

Figure 6: : The critical thermal Rayleigh number of linear theory (solid line) and nonlinear theory (dashed line) plotted against η, where $\varepsilon = \lambda = 0.1$, $\alpha = N_0 = \xi = 1$ and $R_c = 20$.

Figure 7 gives a visual representation of the linear instability and nonlinear stability thresholds, with critical thermal Rayleigh number Ra plotted against R_c and for various α. The remaining parameters are held fixed at $\varepsilon = \lambda = 0.1$ and $N_0 = \xi = \eta = 1$. This figure shows the effect of increasing α on the critical Rayleigh number. It is clear from this figure that an increase in α causes the system to become more stable. For $\alpha = 1,2,3,4$ and 5 and $R_c > 14,20,24,28$ and 32, respectively, the oscillatory convection branch is lowest, leading to this kind of instability at onset.

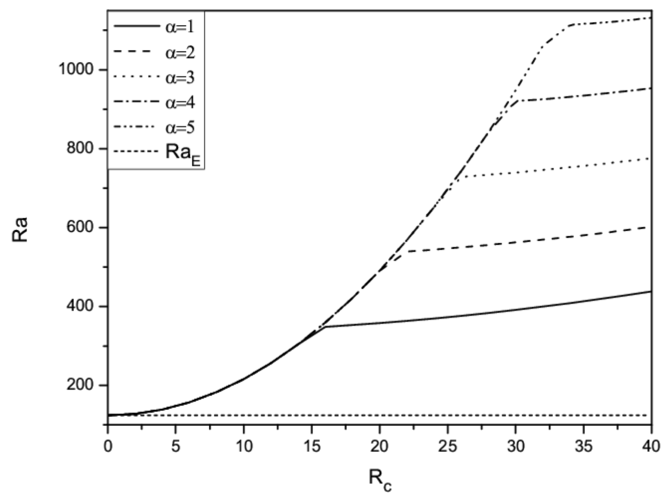

Figure 7: The critical linear thermal Rayleigh number Ra plotted against the solute Rayleigh number R_c, with α varying between 1 and 5, and $\varepsilon = \lambda = 0.1$ and $N_0 = \xi = \eta = 1$.

6 Conclusions

The problem of double diffusive convective movement of a reacting solute in a viscous incompressible occupying a plane layer in a saturated porous medium using Brinkman model has been introduced. We have used the slip boundry coditions planes and no approximation is made in the analysis.The results of linear instability theorem show the area where the instability can occur. The nonlinear theory, which is valid for all initial data, has also been introduced for the model and the thresholds have provided which ensure the global stability when the Rayleigh number is less than these thresholds. The nonlinear thresholds which have been found here, are not close to those of linear theory, thus, we can conclude that the linear instability theory is not accurate in predicting the onset of convective motion. This is important since the virtual appearance of subcritical instabilities guarantees that linearised instability theory does not capture the physics of the onset of convection. Figures 2, 3 and 6, refers to the stabilizing effect of ε, λ and η, respectively. However, Figures 4 and 5 show the stabilizing effect of increasing N_0 and ξ, respectively.

References

[1] J.S. Turner, Buoyancy Effects in Fluids, Cambridge University Press, London, 1973.
[2] J.S. Turner, Double diffusive phenomena, Annu. Rev. Fluid Mech. 6 (1974) 37-56.
[3] J.S. Turner, Multicomponent convection, Annu. Rev. Fluid. Mech. 17 (1985) 11-44.
[4] H.E. Huppert, J.S. Turner, Double diffusive convection, J. Fluid Mech. 106 (1981) 299-329.
[5] J.K. Platten, J.C. Legros, Convection in Liquids, Springer, Berlin, 1984.
[6] A. J. Harfash, Convection in a porous medium with variable gravity field and magnetic field effects, Transp. Porous Media 103 (2014) 361-379.
[7] A.J. Harfash, Magnetic effect on convection in a porous medium with chemical reaction effect, Transp. Porous Media 106 (2015) 163-179.
[8] A.J. Harfash, A. K. Alshara, Chemical reaction effect on double diffusive convection in porous media with magnetic and variable gravity effects, The Korean Journal of Chemical Engineering 32 (2015) 1046-1059.
[9] A.J. Harfash, Three dimensional simulations and stability analysis for convection induced by absorption of radiation, International Journal of Numerical Methods for Heat and Fluid Flow 25 (2015) 810-824.
[10] A.J. Harfash, A. K. Alshara, Magnetic field and throughflow effects on double-diffusive convection in internally heated anisotropic porous media, The Korean Journal of Chemical Engineering 32 (2015) 1970-1985.
[11] A.J. Harfash, A.K. Alshara, A direct comparison between the negative and positive effects of throughflow on the thermal convection in an anisotropy and symmetry porous medium, Zeitschrift Fur Naturforschung A 70 (2015) 383-394 .
[12] A.J. Harfash, Three dimensional simulations for convection induced by the selective absorption of radiation for the Brinkman model, Meccanica. 51 (2016) 501-515.
[13] A.J. Harfash, A.K. Alshara, On the stationary and oscillatory modes of triply resonant penetrative convection, International Journal of Numerical Methods for Heat and Fluid Flow 26 (2016) 1391 - 1415.
[14] A.J. Harfash, Resonant penetrative convection in porous media with an internal heat source/sink effect, Appl. Math. and Computation 281 (2016) 323-342.
[15] A.J. Harfash, Stability analysis for penetrative convection in a fluid layer with throughflow, International Journal of Modern Physics C 27 (2016) 1650101.
[16] A.J. Harfash, Nonhomogeneous Porosity and Thermal Diffusivity Effects on a Double-Diffusive Convection in Anisotropic Porous Media, International Journal of Nonlinear Sciences and Numerical Simulation 17 (2016) 205–220.
[17] A.J. Harfash, F.K. Nashmi, Triply resonant double diffusive convection in a fluid layer, Mathematical Modelling and Analysis 22 (2017) 809-826.
[18] A.J. Harfash, H. A. Challoob, Slip boundary conditions and through flow effects on double-diffusive convection in internally heated heterogeneous Brinkman porous media, Chinese Journal of Physics 56 (2018) 10-22.
[19] M.C. Kim, Nonlinear numerical simulation on the onset of Soret-driven motion in a silica nanoparticles suspension, Korean Journal of Chemical Engineering 30 (2013) 831-835.
[20] B. Straughan, Stability and wave motion in porous media, Series in Applied Mathematical Sciences, vol. 165, Springer, 2008.

[21] D.A. Nield, A. Bejan, Convection in Porous Media, 4th ed., Springer-Verlag, New York, 2013.
[22] C.L.M.H. Navier, Mémoire sur les lois du mouvement des fluides, Mémoires de l'Acad´emie Royale des Sciences d l'Institut de France 6 (1823) 389-440.
[23] B. Straughan, The energy method, stability, and nonlinear convection, Applied Mathematical Sciences, second ed., vol. 91, Springer, 2004.
[24] S. Chandrasekhar, Hydrodynamic and hydromagnetic stability, Dover, New York, 1981.
[25] D.D. Joseph, Uniqueness Criteria for the Conduction-Diffusion Solution of the Boussinesq Equations, Arch. Rational Mech. Anal. 35 (1969) 169-177 .

تأثير رد الفعل الكيميائي على الاستقرار وعدم الاستقرار للحمل الحراري المزدوج في طبقة متوسطة مسامية :نموذج برينكمان

هدى عبد الجبار جلوب، فهد كامل نشمي ، عقيل جاسم حرفش
قسم الرياضيات ، كلية العلوم ، جامعة البصرة ، البصرة ، العراق

المستخلص

مشكلة الحمل المزدوج الانتشار في وسط مسامي مشبع بالمذاب ذات رد الفعل الكيميائي تمت دراستها باستخدام نموذج برينكمان في هذه المقالة. تم تحليل تأثير شروط حدود الانزلاق على عدم استقرار واستقرار هذا النموذج . اعتمادنا النظرية الخطية لعدم الاستقرار والنظرية غير الخطية لدراسة حدود استقرار النموذج. حدود الاستقرار وعدم الاستقرار للنموذج تم تحليلها وتحديد قيمة عدد رايلي كدالة لمعامل الانزلاق. هذه الدراسة اوضحة تأثير تضمين معدل رد الفعل الكيميائي ومعامل برينكمان على عدم استقرار واستقرار النموذج. علاوة على ذلك، التحقق من تاثير معامل القصور الذاتي على حدود عدم الاستقرار الخطية انجز في هذا البحث.